Analog Robust Repetitive Control for Nanopositioning Using Bucket Brigade Devices

Arnfinn A. Eielsen * **J. Tommy Gravdahl** * **Kam K. Leang** **

* *Department of Engineering Cybernetics, Norwegian University of Science and Technology, Trondheim, Norway, (e-mail: {eielsen,tomgra}@itk.ntnu.no)*
** *Department of Mechanical Engineering, University of Nevada – Reno, Reno, NV 89557, USA, (e-mail: kam@unr.edu)*

Abstract: In many applications of nanopositioning, such as scanning probe microscopy, tracking fast periodic reference trajectories with high accuracy is highly desirable. Repetitive control is a simple and effective control scheme to obtain good tracking of such reference trajectories. In order to implement repetitive control, a method for introducing time-delay is necessary. This can easily be implemented using a memory buffer with digital signal processing equipment. To achieve fast, high accuracy, and low noise performance, fast microcontrollers or field-programmable gate array hardware with fast high-resolution analog-to-digital and digital-to-analog converters are needed. As an inexpensive alternative to digital signal processing, the use of an analog bucket brigade device to implement the time-delay is investigated in this paper. Bucket brigade devices use switching to carry the input voltage over an array of capacitors, achieving a specified time-delay. Low-noise bucket brigade devices can achieve a signal-to-noise ratio around 80 dB, comparable to the actual performance when using 16-bit analog-to-digital converters. In this paper, the proposed control scheme utilizes a modified integral control law in conjunction with the repetitive control law. The overall control scheme ensures robustness towards plant uncertainty. Experimental results demonstrate the effectiveness of the overall control scheme and the analog implementation.

1. INTRODUCTION

Nanopositioners employed in applications that include scanning probe microscopy (SPM) require tracking of fast periodic reference trajectories with high accuracy (Salapaka and Salapaka, 2008; Clayton et al., 2009). Periodic reference trajectories occur in both imaging and manipulation applications of SPM equipment. Recently, repetitive control (RC) has been introduced for nanopositioning systems (Aridogan et al., 2009; Merry et al., 2011; Shan and Leang, 2012b). The RC scheme is based on the internal model principle (Francis and Wonham, 1976) and it is specifically tailored to track periodic reference trajectories. At the heart of the control law is a signal generator that provides high gain at the harmonics of the reference trajectory. RC can easily be implemented digitally using a pure time-delay, a memory buffer, inside of a positive feedback loop (Inoue et al., 1981). Compared to traditional feedback and feedforward control laws (Clayton et al., 2009; Devasia et al., 2007), the tracking error of RC diminishes as the number of operating periods increases. The control law generally requires only the period of the reference trajectory to be known (Inoue et al., 1981). An important feature of RC is that as long the overall control loop is stable, the RC scheme is invariant to changes in plant dynamics, thus the achieved performance should be consistent for any plant perturbations within the specifications of the chosen uncertainty weight. In many nanopositioning applications, the period of the reference signal is known in advance which makes RC attractive. Compared to iterative learning control (ILC) (Moore et al., 1992; Bristow et al., 2008; Wu and Zou, 2007; Leang and Devasia, 2006), RC does not require resetting the initial conditions at the start of each iteration step, and has less computational complexity. It is pointed out that ILC for hysteretic systems require a cycling process to reset the initial conditions at the beginning of each iteration (Leang and Devasia, 2006). For convenience, an RC can be plugged into an existing feedback loop to enhance performance.

A digital implementation of an RC scheme for nanopositioning puts some requirements on the hardware used. To obtain high accuracy and low noise, the analog-to-digital converters (ADCs) and digital-to-analog converters (DACs) used must feature high resolution and must be capable of high sampling frequencies. High resolution is required to have a reasonable lower bound for the absolute achievable accuracy, and to minimize the effects of quantization noise. A high sampling frequency is necessary to sample at a sufficient rate with respect to the bandwidth of dominant dynamics of the controlled system, and also to minimize the power spectral density of the quantization noise in the sampled signal. This means that microcontrollers or field-programmable gate arrays used for the digital signal processing must be able to handle high data rates, as well as support floating point arithmetic or a large word size for fixed point arithmetic. Programming the required filtering algorithms for microcontrollers or field-programmable gate arrays can also be time-consuming, and often requires proprietary compilers. The implementation can be simplified by using ready-made hardware-in-the-loop systems, albeit at a higher overall cost for the system.

This paper investigates the use of analog filters and an analog bucket brigade device (BBD) for the implementation of an analog RC scheme. In terms of required equipment, this is an inexpensive and simpler alternative to digital signal processing.

The BBD is used to implement the necessary time-delay. In a BBD the input signal is sampled in time and passed into a series of capacitors and transistor switches. The charge in each capacitor stage is passed into the subsequent stage at a rate determined by an external clock signal (Sangster and Teer, 1969; Weckler, 1977; Raffel and Smith, 2010). This produces a time-delayed version of an input signal. The BBD is thus a hybrid device, which uses sampling, but not quantization. Low-noise BBDs from the MN3000 series from Panasonic can achieve a signal-to-noise ratio, or dynamic range, from 80 to 90 dB. Using terminology from the analysis of ADCs, this equates to 13 or more effective number of bits (ENOB). This is comparable to the actual performance when using 16-bit ADCs (Walden, 1999). The dynamic range for a BBD can in some cases be improved by using companding (compressing and expanding a signal before and after some operation) (Raffel and Smith, 2010), but this has not been applied in the presented implementation. An alternative to BBDs is charge couple device (CCD) delay lines (Weckler, 1977; Catrysse et al., 1980), but BBDs for designed for audio applications are still in production and available for purchase at the time of writing.

The performance and stability of RC depends on the dynamics of the controlled system (Hara et al., 1988; Inoue, 1990). Particularly, sharp resonance peaks can degrade performance and even make creating a stable RC system difficult. Positioning systems for nanopositioning often involve moving payloads of various masses. The resonance frequencies and the effective control gain of the mechanical structure will therefore change every time a new payload is attached. Because the majority of nanopositioning designs use piezoelectric actuators, inherent variations in the effective control gain due to changes in actuator temperature, offset voltage, displacement range, as well as due to depolarization of the piezoelectric actuator must be taken into account. Piezoelectric actuators also introduce disturbances due to hysteresis and creep. Thus, the presence of hysteresis can also jeopardize the stability of an RC system designed around a linear dynamics model for the plant (Shan and Leang, 2012a).

The use of BBDs for RC have previously been investigated (Escobar et al., 2007; Leyva-Ramos et al., 2005), but using different control law structures. This paper presents a control scheme based on the design proposed in (Eielsen et al., 2012b). The scheme consists of a modified integral control law, combined with a plug-in type RC scheme. When applying the scheme to a nanopositioning stage, the presence of high-gain integral action helps to reduce the sensitivity of the system to the hysteresis and creep nonlinearities inherent in the piezo actuator. The sensitivity due to the dominant resonant response of the positioning stage is also reduced, as the modified integral control law introduces damping. The tuning methodology used for the RC scheme incorporates the uncertainty of the plant, and the uncertainty weight can therefore be tailored to include effects such as changing gain or resonance frequency, as well as other effects, if necessary.

2. SYSTEM DESCRIPTION AND MODELING

The custom-designed nanopositioning stage used in this work is shown in Fig. 1. It is a serial-kinematic motion mechanism designed such that the first vibration mode is dominant and occurs in the actuation direction (piston mode). The simplified free body diagram for the mechanism is displayed in the inset image in Fig. 1, and by this model the corresponding second-order differential equation to describe the dynamics (where subscript "x" indicates the x direction) is given by

$$m_x \ddot{x}_x(t) + c_x \dot{x}_x(t) + k_x x_x(t) = f_x(t) \ , \qquad (1)$$

where m_x (kg) is the mass of the sample platform, as well as any additional mass due an attached payload, c_x (N s m^{-1}) is the damping coefficient, and k_x (N m^{-1}) is the spring constant. The applied external force from the piezoelectric actuator f_x (N) is

$$f_x(t) = \beta u_a(t) + d_h(t) \ , \qquad (2)$$

where β (N V^{-1}) is the effective gain [1] of the piezoelectric actuator from voltage to force, and $u_a(t)$ (V) is the applied voltage. The piezoelectric actuator will introduce hysteresis and creep when driven by a voltage signal. It is a reasonable assumption to consider this behavior as a bounded disturbance added to the input (Eielsen et al., 2012a), represented by the term $d_h(t)$.

Denoting the output $y = x_x$, the transfer function for the nanopositioning stage is

$$G(s) = \frac{y}{u_a}(s) = \frac{b_0}{s^2 + a_1 s + a_0} = \frac{b_0}{s^2 + 2\zeta\omega_0 s + {\omega_0}^2} \ , \qquad (3)$$

where $b_0 = \beta/m$ (m s^{-2} V^{-1}), $a_0 = k/m$ (s^{-2}), $a_1 = c/m$ (s^{-1}), $\zeta = c/2\sqrt{mk}$ (-), and $\omega_0 = \sqrt{k/m}$ (s^{-1}).

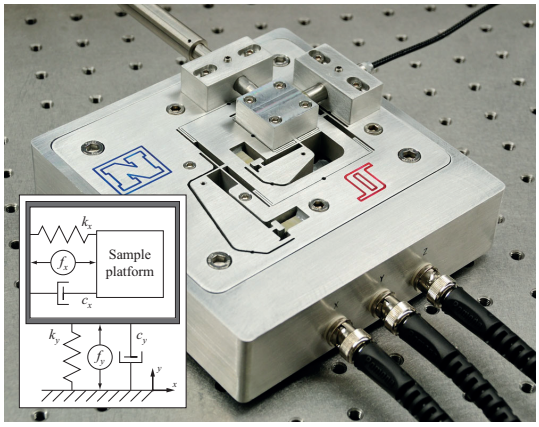

Fig. 1. Experimental serial-kinematic nanopositioning stage.

The measured frequency response for the x axis is displayed in Fig. 2. The input is taken to be the voltage input to the high-voltage piezo amplifier, and the output is the voltage output from the capacitive sensor gauge. The model (3) is fitted to the frequency response data using the MATLAB System Identification Toolbox, and the resulting parameter values are: $b_0 = 9.82 \cdot 10^6$ V/V; $\zeta = 19.6 \cdot 10^{-3}$; and $\omega_0 = 2\pi \cdot 762$ rad/s. The response of the model (3) using these parameters is also displayed in Fig. 2 for comparison.

The actual response of the first vibration mode is well approximated by the second-order model (3). There are higher order modes in the system, but these have negligible magnitude responses in comparison to the first, thus the second-order model is sufficient to describe the dominant dynamics.

The system has uncertainty with regards to the parameters, and the model (3) does not include high frequency dynamics. A reasonable stability margin is therefore needed and the control law must have sufficient attenuation at higher frequencies to

[1] Mainly determined by the material, amount of polarization, and the driving voltage amplitude (as the amount of deflection generated changes with voltage amplitude due to hysteresis).

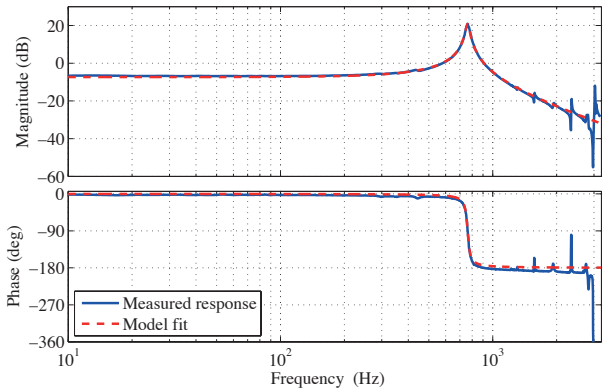

Fig. 2. Measured frequency response (solid line) for x-axis of the nanopositioning stage and the model (3) (dash line).

avoid excitation of the higher frequency dynamics. To assess the robustness of the proposed control scheme, the uncertainty of the system model is taken into account as a multiplicative perturbation to the positioner dynamics, i.e.,

$$G_p(s) = G(s)(1 + w_G(s)\Delta_G(s)); \ |\Delta_G(j\omega)| \leq 1 \ \forall \ \omega \ . \quad (4)$$

The uncertainty weight $w_G(s)$ is determined experimentally, and an approximate over-bound is found. These results are shown in Fig. 3.

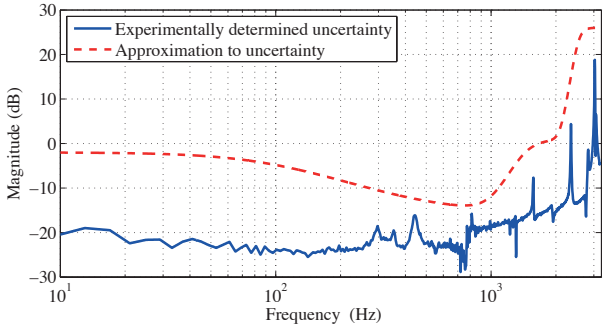

Fig. 3. Open-loop uncertainty weight $w_G(s)$, using experimental data and as over-bounding transfer function.

3. CONTROL LAW DESIGN AND TUNING

The system to which the control scheme is applied consists of the positioning stage, a voltage amplifier, and a capacitive displacement sensor. [2] The control scheme consists of a modified integral control law, and the plug-in repetitive control scheme. The modified integral control law is comprised of a regular integrator, and the anti-aliasing and reconstruction filters. A block diagram for the overall system is shown in Fig. 4.

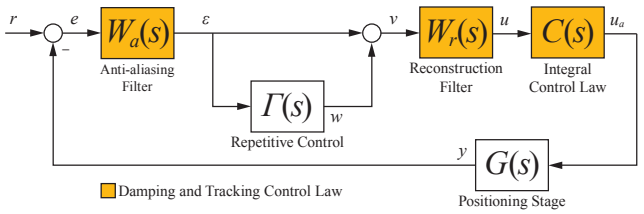

Fig. 4. System block diagram.

[2] As the amplifier and sensor used in the experimental set-up have very fast dynamics, they have been neglected in the system analysis.

3.1 Repetitive Control Scheme

Repetitive control intends to track or reject arbitrary periodic signals of a fixed period T_p, by embedding a model of the reference r or disturbance d signal in the control law. The transfer function for the RC configuration shown in Fig. 5(a) is given as

$$\frac{w}{\varepsilon}(s) = \Gamma(s) = \frac{R(s)\mathrm{e}^{-T_p s}}{1 - Q(s)\mathrm{e}^{-T_p s}} \ , \quad (5)$$

where $Q(s)$ is a unity-gain low-pass filter, and $R(s)$ is an output filter, defined below. It is pointed out that the low-pass filter $Q(s)$ shifts all the poles into the complex left half-plane, with an amount dependent on frequency, so at higher frequencies the pole locations is further away from the original locations than at lower frequencies. This will degrade the nulling property of the control law at the fundamental and harmonic frequencies of the reference signal. Steps to improve on this situation are discussed in Section 3.4.

By inspection of Fig. 4, the closed-loop sensitivity function for the overall system is found as

$$\frac{e}{r}(s) = S(s) = \frac{1}{1 + \bar{G}(s)C(s) + \bar{G}(s)C(s)\Gamma(s)} = \frac{1}{\Delta(s)} \ , \quad (6)$$

where $\bar{G}(s) = W_r(s)G(s)W_a(s)$. The stability of the closed-loop system is determined by the denominator

$$\Delta(s) = 1 + \bar{G}(s)C(s) + \bar{G}(s)C(s)\Gamma(s) \ . \quad (7)$$

Now, consider the sensitivity $\bar{S}(s)$ and complementary $\bar{T}(s)$ sensitivity function excluding the RC scheme

$$\bar{S}(s) = \frac{1}{1 + C(s)\bar{G}(s)} \ \text{ and } \ \bar{T}(s) = C(s)\bar{G}(s)\bar{S}(s). \quad (8)$$

Then, by inserting the expression for $\Gamma(s)$, multiplying the numerator and denominator of $1/\Delta(s)$ by $\bar{S}(s)$, and rearranging, the sensitivity function for the closed-loop system when adding the repetitive control law becomes

$$S(s) = \frac{1}{\Delta(s)} = \frac{\bar{S}(s)(1 - Q(s)\mathrm{e}^{-T_p s})}{1 - (Q(s) - \bar{T}(s)R(s))\mathrm{e}^{-T_p s}} \ . \quad (9)$$

With reference to Fig. 5(b), it can be seen that given a bounded reference $r(t)$ and stable transfer functions $\bar{S}(s)$ and $Q(s)$, the small-gain theorem provides the criterion for the stability of the closed-loop system as (Hara et al., 1988)

$$\left\| Q(s) - \bar{T}(s)R(s) \right\|_\infty < 1 = 0 \text{ dB} \ , \quad (10)$$

where it is noted that $|\mathrm{e}^{-jT_p\omega}| = 1 \ \forall \ \omega \in \mathbb{R}$.

The output filter $R(s)$ is constructed as

$$R(s) = {W_T}^{-1}(s)Q(s) \ , \quad (11)$$

introducing a stable all-pole filter $W_T(s)$, which provides for some flexibility in meeting the stability criterion. Using a unity-gain low-pass filter $Q(s)$, the following somewhat simpler criterion

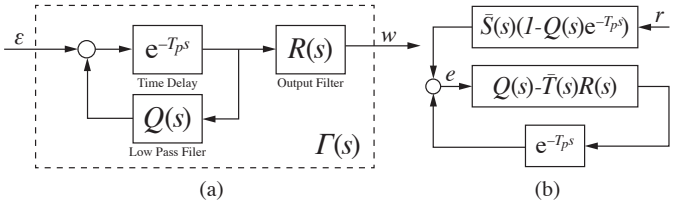

Fig. 5. (a) Plug-in repetitive control scheme. (b) Equivalent representation of the sensitivity function Eq. (9).

$$\left\| 1 - {W_T}^{-1}(s)\bar{T}(s) \right\|_\infty < 1 = 0 \text{ dB} \tag{12}$$

can be used for selecting an appropriate filter $W_T(s)$.

To assess the robustness of the RC, a multiplicative perturbation for the closed loop complementary sensitivity is used, that is:

$$\bar{T}_p(s) = \bar{T}(s)(1 + w_T(s)\Delta_T(s));\ 0 < |\Delta_T(j\omega)| \leq 1\ \forall\ \omega\ . \tag{13}$$

An estimate for the closed-loop uncertainty weight $w_T(s)$ can be found using

$$\bar{T}(s)(1 + w_T(s)\Delta_T(s)) = \frac{C(s)\bar{G}(s)(1 + w_G(s)\Delta_G(s))}{1 + C(s)\bar{G}(s)(1 + w_G(s)\Delta_G(s))}\ .$$

Recalling that $\bar{S}(s) + \bar{T}(s) = 1$ and the triangle inequality, one can then find that

$$w_T(s)\Delta_T(s) = \frac{\bar{S}(s)w_G(s)\Delta_G(s)}{1 + \bar{T}(s)w_G(s)\Delta_G(s)} \ \Rightarrow \ |w_T(j\omega)| \leq |\bar{S}(j\omega)w_G(j\omega)|\ . \tag{14}$$

Incorporating the uncertainty into the criterion (10) and applying the triangle inequality, a robust stability criterion is obtained:

$$\left|Q(j\omega) - \bar{T}(j\omega)R(j\omega)\right| < 1 - \left|\bar{T}(j\omega)w_T(j\omega)R(j\omega)\right|\ . \tag{15}$$

3.2 Modified Integral Control Law

The nanopositioning stage is a lightly damped structure as shown by the measured frequency response in Fig. 2. Inspecting the stability criterion for the repetitive control scheme, one can expect that large peaks in the complementary sensitivity function $\bar{T}(s)$ can reduce the applicable bandwidth and gain for the repetitive control law, depending on how well the output filter $R(s)$ is able to match the inverse closed-loop dynamics. Introducing a robust damping and tracking control law increase the robustness and bandwidth for the overall control scheme.

A simple, effective, and robust damping and tracking control law for a lightly damped structure can be obtained by modifying and optimally tuning an integral control law (Eielsen et al., 2014). Since the BBD is a sampled device, reconstruction and anti-aliasing filters must be present in order to mitigate aliasing effects. As the external clock signal driving the BBD bleed into the output signal, the reconstruction filter also serves to attenuate the clock signal noise. By including these filters, an extra degree of freedom is added for the tuning of the control law, i.e., the cut-off frequency of the filters. Since reconstruction and anti-aliasing filters must be present, this particular control law structure provides a minimal physical realization, which also uses the filters to good effect. Compared to a regular integral control law the modified integral control law will introduce damping, thus enabling an increased bandwidth. The integral action also serves to suppress the hysteresis and creep nonlinearities.

An integral control law is given as

$$C(s) = \frac{k_i}{s}\ , \tag{16}$$

where k_i is the integral gain. Here the filters are taken to be first-order low-pass filters

$$W_a(s) = W_r(s) = \frac{\omega_c}{s + \omega_c}\ , \tag{17}$$

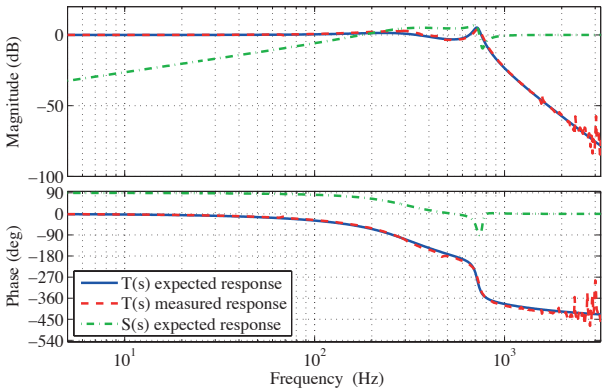

Fig. 6. Amplitude and phase response for the complementary sensitivity $\bar{T}(s) = y(s)/r(s)$ and sensitivity $\bar{S}(s) = e(s)/r(s)$ when using the modified integral law.

where ω_c is the cut-off frequency. For convenience they are taken to be identical when tuning the control law. The modified integral control law is therefore

$$\bar{C}(s) = W_a(s)C(s)W_r(s)\ . \tag{18}$$

As discussed in (Eielsen et al., 2014), the optimal values for the cut-off frequency and the integral gain can be found by minimizing

$$J_C(k_i, \omega_c) = \left\| 1 - \left|\bar{T}(k_i, \omega_c; j\omega)\right| \right\|_2\ , \tag{19}$$

where $\|\cdot\|_2$ denotes the L^2-norm, truncated as needed. The minimization of (19) attempts to produce the flattest possible response for the complementary sensitivity function.

Evaluating the cost-function (19) results in

$$[{k_i}^\star,\ {\omega_c}^\star] = \arg\min_{k_i, \omega_c} \left[J_C(k_i, \omega_c)\right] \text{ s.t. } \mathrm{Re}\left\{\lambda_i\right\} \in \mathbb{R}^- \wedge k_i \in \mathbb{R}^+ \wedge \omega_c \in \mathbb{R}^+/\{0\} \approx [3070,\ 2\pi \cdot 572 \text{ rad s}^{-1}]\ ,$$

where λ_i are the eigenvalues of the closed-loop system.

The resulting frequency responses for the complementary sensitivity and sensitivity for the optimal configuration are displayed in Fig. 6. The optimal tuning effectively attenuates the resonant mode, and by inspection of the sensitivity function response in Fig. 6 the closed-loop bandwidth can be determined to be approximately 100 Hz.

The robustness of the integral control law with regards to the uncertainties displayed in Fig. 3 is determined. The criterion (Skogestad and Postlethwaite, 2005)

$$\|w_G(s)\bar{T}(s)\|_\infty < 1 = 0 \text{ dB} \tag{20}$$

is evaluated, and the results are shown in Fig. 7.

3.3 Choosing $R(s)$ and $Q(s)$

Considering the stability criterion for the repetitive control law (12), the ideal choice for the included filter would be $W_T(s) = \bar{T}(s)$, as this would produce the minimum of the norm (12). A sufficient choice for $W_T(s)$ would be a filter that attenuates $\bar{T}(s)$ sufficiently to meet the stability criterion, as tracking performance is independent of the dynamics of the controlled plant due to the nulling properties of RC.

The complementary sensitivity function $\bar{T}(s)$ has relative degree $n_r = 5$. As the closed loop response of the system using the modified integral control law is fairly flat, $W_T(s)$ is chosen

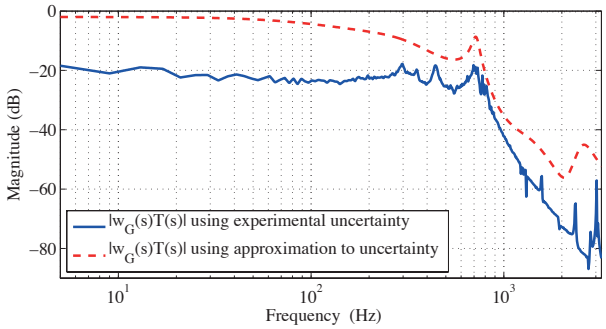

Fig. 7. Evaluation of robust stability criterion $|w_G(j\omega)\bar{T}(j\omega)|$ for the modified integral control law.

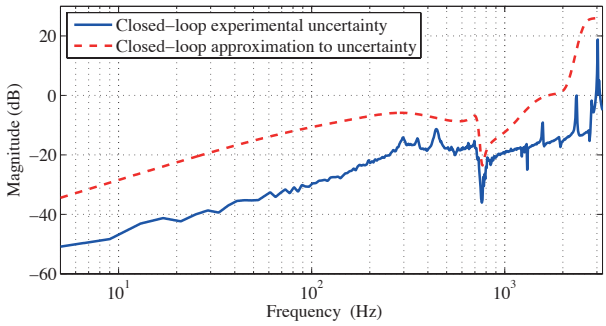

Fig. 8. Closed-loop uncertainty weight $w_T(s)$, using experimental data and as an over-bounding transfer function.

to be a fifth-order Butterworth filter with DC-gain k_T, and it is assumed that $W_T(s) \approx \bar{T}(s)$. An optimal choice for the cut-off frequency ω_T and DC-gain k_T for $W_T(s)$ is found minimizing the cost-function

$$J_T(k_T, \omega_T) = \sup\{|Q(j\omega) - \bar{T}(j\omega)R(\omega_T, k_T; j\omega))| + |\bar{T}(j\omega)w_T(j\omega)R(\omega_T, k_T; j\omega))| : \omega \in \mathbb{R}\}\,, \quad (21)$$

where $R(j\omega, \omega_T, k_T) = W_T(j\omega, \omega_T, k_T)^{-1}Q(j\omega)$. The evaluation of the cost-function must satisfy $J_T(k_T^\star, {\omega_T}^\star) < 1$ in order for the system to be robustly stable.

The filter $Q(s)$ must be chosen before performing the optimization. This is done with consideration to the filter $R(s)$, and chosen to be a unity-gain fifth-order Butterworth filter, such that $R(s) = {W_T}^{-1}(s)Q(s)$ is a proper filter.[3] By inspection of the frequency response in Fig. 2, a cut-off frequency for $Q(s)$ can be chosen in order to attenuate the second and higher order vibration modes, in order to satisfy (15). A cut-off frequency of $2\pi \cdot 2500$ rad/s would seem adequate, but due to the tolerances of the components used and the high sensitivity to component values for the zeros in the state-variable filter used in the implementation, a cut-off frequency of $\omega_Q = 2\pi \cdot 1750$ rad/s was used in order to improve robustness. Minimizing (21) yielded the optimal values $k_T^\star \approx 0.25$ and ${\omega_T}^\star \approx 2\pi \cdot 590$.

The closed-loop uncertainties used are shown in Fig. 8, and the evaluation of (15) is shown in Fig. 9.

3.4 The Effect of $Q(s)$ on RC Pole Locations

Due to the low-pass filter $Q(s)$, perfect tracking is not possible, since the nulling property of RC is determined by

$$\mathcal{L}^{-1}\left[(1 - Q(s)\mathrm{e}^{-T_p s})r(s)\right] = r(t) - \tilde{r}(t - T_p) \quad (22)$$

[3] By this particular choice, $W_T(s)$ and $Q(s)$ being all-pole filters, $R(s)$ and $Q(s)$ can be realized using a single filter with two outputs, as shown in Sec. 4.2.

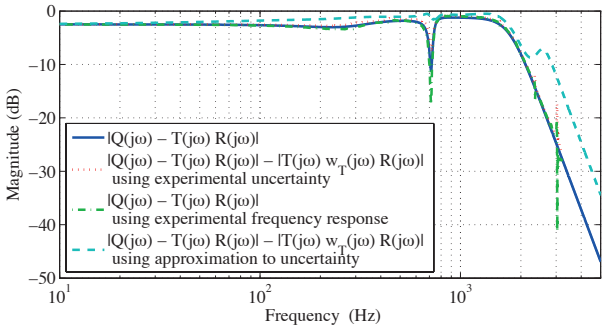

Fig. 9. Numeric evaluation of stability criteria (10) and (15).

where $\tilde{r}(t) = Q(t) * r(t) \neq r(t)$. It is possible to modify the time-delay T_p to partially compensate for the shift in the poles due to $Q(s)$. For the analog implementation, since the exact value of T_p is dependent on the tolerances of components used, the simplest solution is to adjust the fundamental frequency of the reference signal in order to minimize the stationary root-mean-square value of the error signal.

4. IMPLEMENTATION

The implementation of the control scheme consists of three parts, the time-delay, the modified integral control law, and the $Q(s)$ and $R(s)$ filters. The interconnection between these parts is shown in Fig. 10, and the actual implementation is shown in Fig. 11. In addition to the BBD, the necessary filters were implemented using standard operational amplifier circuits. All the circuits used the OPA227 operational amplifier, but the lower specification TL081 was also successfully tested.

4.1 Realization of Time-Delay

The circuit implementing the time-delay is shown in Fig. 12. The time-delay T_p in the BBD is determined as

$$T_p = \frac{N}{2f_{cp}} \quad (23)$$

where N is the number of stages in the BBD and f_{cp} is the frequency of the external clock signal (Weckler, 1977). For the BBD used in the implementation, Panasonic MN3007, $N = 1024$. As the BBD is a unipolar device with a non-unity gain, the signal must be shifted and scaled before and after passing through the BBD. The shifting and scaling is adjusted using R_{oif}, R_{oi}, R_{oof}, and R_{oo}. The output of the BBD has a first-order low-pass filter with a cut-off frequency of approximately $(2\pi \cdot 5 \cdot 10^3 \cdot 330 \cdot 10^{-12})^{-1} = 96.5$ kHz to remove some of the clock signal noise. The frequency f_{cp} can be adjusted monitoring either the CP1 or CP2 output of the MN3101 clock gen-

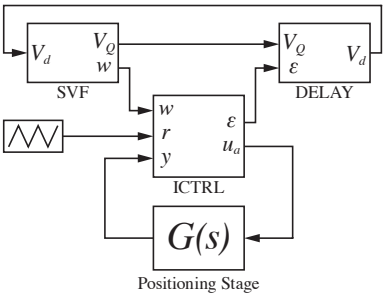

Fig. 10. Interconnection of the different components of the implemented circuits, cf. Figs. 12, 13, and 14.

erator on an oscilloscope, while adjusting the resistance value R_{ox2}.

4.2 Realization of Modified Integral Control Law

The modified control law is implemented as shown in Fig. 13. The anti-aliasing and reconstruction filters are first-order low-pass, and the cut-off frequency ω_c is determined by adjusting R_{f1} and R_{f2} to satisfy

$$\omega_c = \frac{1}{R_{f1}C_{f1}} = \frac{1}{R_{f2}C_{f2}} \,. \tag{24}$$

The integral control law gain is determined, assuming $R_{e1} = R_{e2} = R_{ef} = R_{eg}$ and $R_{s1} = R_{s2}$ and $R_{sf} = R_{sg}$, by adjusting R_{kf} to satisfy

$$k_i = \frac{R_{kf}}{R_{ki}} \frac{1}{R_i C_i} \,. \tag{25}$$

4.3 Realization of State-Variable Filter

By following the development in (Kerwin et al., 1967), it is relatively straight forward to derive the topology for a state-variable filter which implements the general proper transfer-function

$$\frac{Y(s)}{U(s)} = \frac{b_0 s^n + b_1 s^{n-1} + \ldots + b_{n-1}s + b_n}{s^n + a_1 s^{n-1} + \ldots + a_{n-1}s + a_n} \,,$$

which must be assumed to be stable. Fig. 14 displays the fifth-order filter required to implement $Q(s)$ and $R(s)$. As $R(s) = {W_T}^{-1}(s)Q(s)$, and since $W_T(s)$ and $Q(s)$ are all-pole filters, $Q(s)$ and $R(s)$ can be realized using a single filter with two outputs.

The network analysis of the topology in the time-domain closely resembles a system on controllable canonical form, and thus it is straight forward to find the mapping from the coefficients $\{a_i\}$ and $\{b_0, b_i\}$, to the resistance values $\{R_i\}$, $\{R_{z0}, R_{zi}\}$, $i \in \{1, 2, 3, 4, 5\}$.

Denoting the time-constant for each integrator in the filter as

$$\tau_i = R_i C_i \,, \tag{26}$$

the resistance values $\{R_i\}$ determining the poles are found using:

$$a_1 = \frac{1}{\tau_1} \,,\; a_2 = \frac{a_1}{\tau_2} \,,\; a_3 = \frac{a_2}{\tau_3} \,,\; a_4 = \frac{a_3}{\tau_4} \,,\; a_5 = \frac{a_4}{\tau_5}$$

The zeros of the filter are determined by the resistance values of $\{R_{z0}, R_{zi}\}$. Defining

$$G_p = \frac{1}{R_{z1}} + \frac{1}{R_{z3}} + \frac{1}{R_{z5}} + \frac{1}{R_{g1}} \,,$$

$$G_n = \frac{1}{R_{z2}} + \frac{1}{R_{z4}} + \frac{1}{R_{z0}} \,,$$

$$K_p = \frac{1 + R_{f1}G_n}{G_p} \quad \text{, and} \quad K_n = -R_{f1} \,,$$

the required resistance values can be found solving:

$$\begin{bmatrix} K_p/R_{z1} + (R_{bf}/R_{bi})\tau_1 \,(b_5 - a_5 b_0) \\ K_n/R_{z2} + (R_{bf}/R_{bi})\tau_1\tau_2 \,(b_4 - a_4 b_0) \\ K_p/R_{z3} + (R_{bf}/R_{bi})\tau_1\tau_2\tau_3 \,(b_3 - a_3 b_0) \\ K_n/R_{z4} + (R_{bf}/R_{bi})\tau_1\tau_2\tau_3\tau_4 \,(b_2 - a_2 b_0) \\ K_p/R_{z5} + (R_{bf}/R_{bi})\tau_1\tau_2\tau_3\tau_4\tau_5 \,(b_1 - a_1 b_0) \\ K_p/R_{z0} + (R_{bf}/R_{bi})b_0 \end{bmatrix} = \mathbf{0} \,. \tag{27}$$

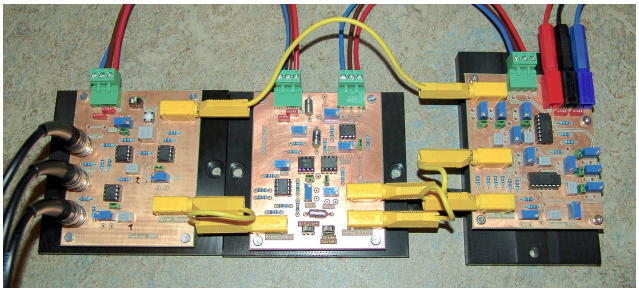

Fig. 11. Implemented repetitive control scheme.

In the general case, depending on the exact values for the poles and zeros, it might be necessary to modify the output summation stage generating the signal w, in order to find a realizable filter.

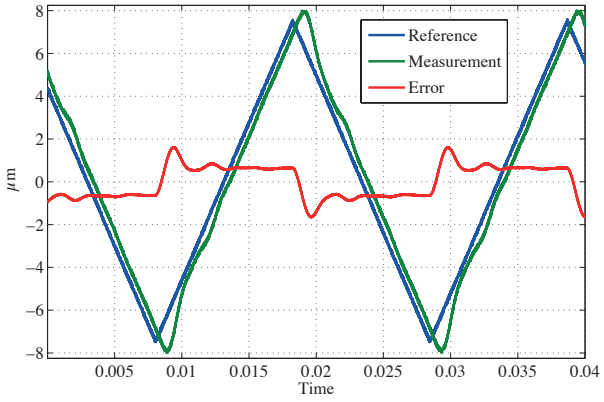

Fig. 15. Stationary tracking results using modified integral law.

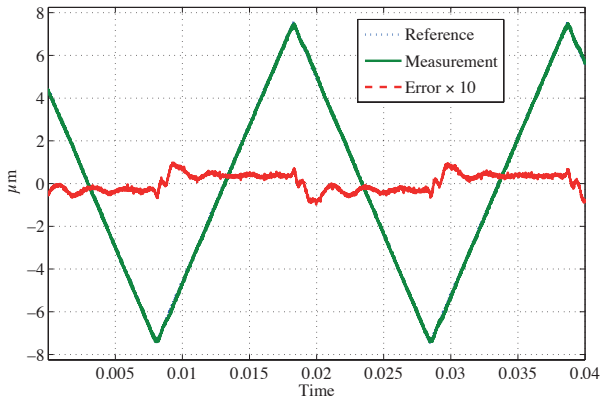

Fig. 16. Stationary tracking results using repetitive control scheme. Note that the error has been multiplied by a factor of 10.

5. EXPERIMENTAL RESULTS

5.1 Description of the Experimental System

In addition to the components already described, an Agilent 33220A function generator was used to generate the reference signal, and a Tektronix TDS 3014C oscilloscope was used to record the results. An ADE 6501 capacitive probe and ADE 6810 gauge was used to measure the mechanical displacement, and a PiezoDrive PDL200 voltage amplifier was used to drive the piezoelectric actuator.

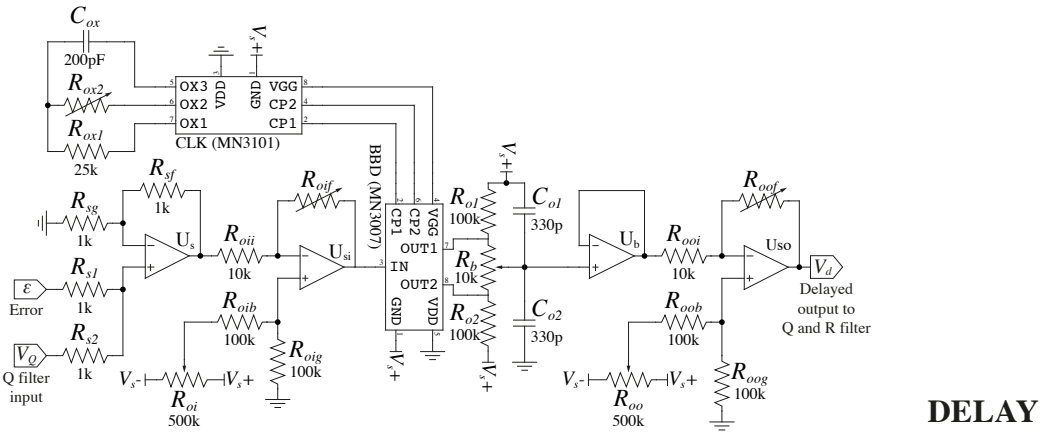

Fig. 12. Time-delay circuit.

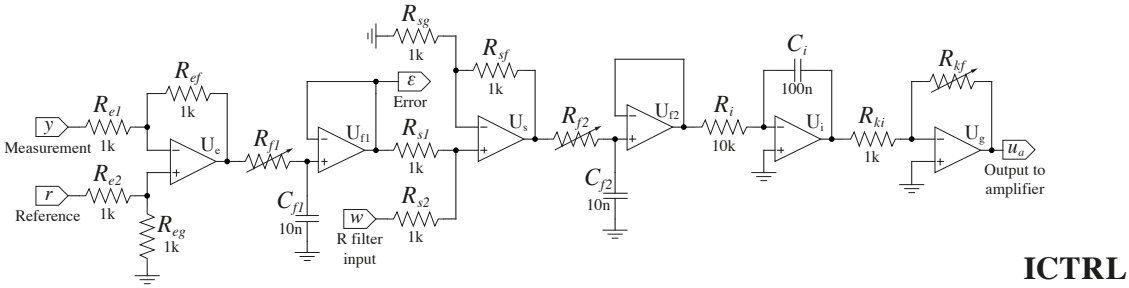

Fig. 13. Integral control law, anti-aliasing and reconstruction filter, and summation circuit.

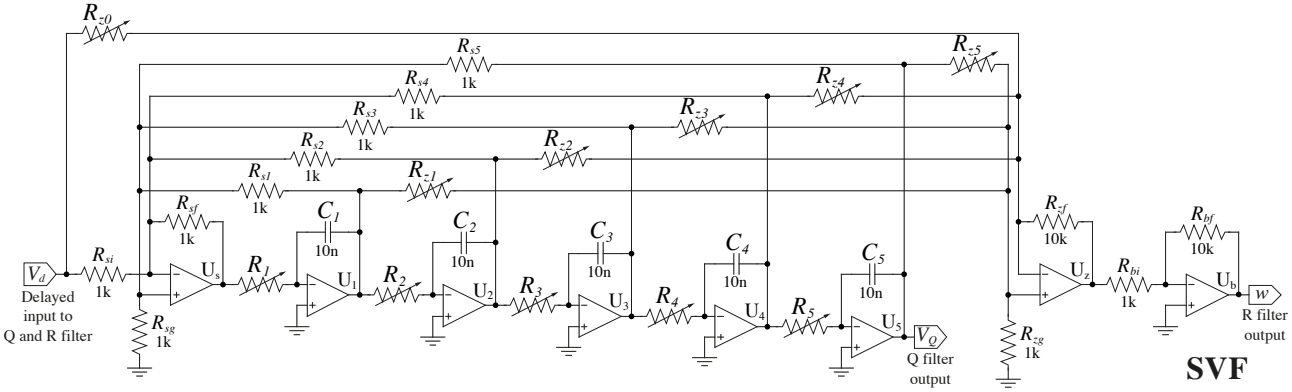

Fig. 14. Circuit for a state-variable filter with fives states, generating five poles and five zeros.

5.2 Results

Results from the experiments are presented in Figs. 15 and 16 when applying a triangle-wave reference signal with period $T_p = 0.02$ s. The plots show the stationary response of the measured deflection $y(s)$ and error $\varepsilon(s) = W_a(s)r(s) - y(s)$.

When applying the modified integral law only, the maximum stationary error is 1.62 μm (21%), and when applying the RC scheme, the maximum stationary error reduced to 0.100 μm (2.2%).

6. DISCUSSION

Applying the modified integral law introduces damping, and integral action suppresses hysteresis and creep. This greatly reduces the sensitivity of the system, i.e. the plant uncertainty is reduced, cf. Figs. 3 and 8. This makes it possible to achieve higher bandwidth for the plug-in repetitive control scheme. One salient problem with the implementation, however, is that the state-variable filter topology has high sensitivity to component values in the summer which generates the zero. The solution used in this paper was to reduce the bandwidth of the RC scheme, i.e. the cut-off frequency of the $Q(s)$ filter.

The tracking performance for the RC scheme is determined by the bandwidth of the $Q(s)$ filter, thus, in order to increase the tracking performance, components with better tolerances should be used, and the uncertainty introduced by the $Q(s)$ and $R(s)$ filters should be incorporated into the uncertainty weight, to obtain a more reliable tuning result. It can be mentioned that an equivalent digital implementation was done using a dSPACE DS1103 hardware-in-the-loop system, where the bandwidth of the $Q(s)$ filter was increased to $2\pi \cdot 2000$ rad/s, and the error was reduced by about one order of magnitude. Thus improving the precision of the filters should translate to an improved tracking performance.

With regards to the BBD, the main problem is the clock noise. A reconstruction filter with sufficient attenuation at and above the driving clock signal frequency is required. This can therefore preclude the usage of BBD based RC schemes for very high-

bandwidth positioning stages, as well as the application of very low-frequency reference signals.

7. FUTURE WORKS

In order to improve the tracking performance, a state-variable filter with high-precision components should be used, and the uncertainty introduced by the various filters due to component tolerances should be accounted for explicitly in the uncertainty weights. Improvement in dynamic range in the BBD when using a compander circuit should be investigated.

8. CONCLUSIONS

This paper focused on the design and implementation of an analog repetitive control scheme using a bucket brigade device. The experimental results showed good tracking performance for an experimental nanopositioning system. The chosen design features low-order filters, which are feasible for implementation using standard operational amplifier circuits, but is also able to handle a fair amount of uncertainty. This results in a low component count, and since the bucket brigade device has comparable dynamic range to high-resolution DACs, the proposed implementation can be used as an inexpensive alternative to digital signal processing solutions. The proposed scheme can also be implementable on existing hardware configurations for nanopositioning, as it should require only minor modifications to a standard configuration.

REFERENCES

Aridogan, U., Shan, Y., and Leang, K.K. (2009). Design and analysis of discrete-time repetitive control for scanning probe microscopes. *ASME J. Dyn. Syst. Meas. and Cont.*, 131, 061103 (12 pages).

Bristow, D.A., Dong, J., Alleyne, A.G., Ferriera, P., and Salapaka, S. (2008). High bandwidth control of precision motion instrumentation. *Rev. Sci. Instr.*, 79, 103704.

Catrysse, J.A., Declerck, G., and De Meyer, C.C. (1980). CCD Delay Lines in Audio. *Journal of the Audio Engineering Society*, 28(11), 800–808.

Clayton, G.M., Tien, S., Leang, K.K., Zou, Q., and Devasia, S. (2009). A review of feedforward control approaches in nanopositioning for high speed SPM. *ASME J. Dyn. Syst. Meas. and Cont.*, 131(6), 061101 (19 pages).

Devasia, S., Eleftheriou, E., and Moheimani, S.O.R. (2007). A survey of control issues in nanopositioning. *IEEE Trans. Cont. Syst. Tech.*, 15(5), 802 – 823.

Eielsen, A.A., Gravdahl, J.T., and Pettersen, K.Y. (2012a). Adaptive feed-forward hysteresis compensation for piezoelectric actuators. *Rev. Sci. Instrum.*, 83(8), 085001.

Eielsen, A.A., Leang, K.K., and Gravdahl, J.T. (2012b). Robust Damping PI Repetitive Control for Nanopositioning. In *Proc. American Control Conference*, 3803–3810. Montreal.

Eielsen, A.A., Vagia, M., Gravdahl, J.T., and Pettersen, K.Y. (2014). Damping and Tracking Control Schemes for Nanopositioning. *IEEE/ASME Trans. Mechatronics*, 19(2), 432–444.

Escobar, G., Martinez, P.R., and Leyva-Ramos, J. (2007). Analog Circuits to Implement Repetitive Controllers With Feedforward for Harmonic Compensation. *IEEE Trans. Ind. Electron.*, 54(1), 567–573.

Francis, B.A. and Wonham, W.M. (1976). The internal model principle of control theory. *Automatica*, 12(5), 457 – 465.

Hara, S., Yamamoto, Y., Omata, T., and Nakano, M. (1988). Repetitive control system: a new type servo system for periodic exogenous signals. *IEEE Trans. Autom. Control*, 33(7), 659–668.

Inoue, T. (1990). Practical repetitive control system design. In *Proceedings of the 29th IEEE Conference on Decision and Control*, volume 3, 1673 – 1678.

Inoue, T., Nakano, M., and Iwai, S. (1981). High accuracy control of a proton synchrotron magnet power supply. In *Proc. 8th World Congr. IFAC*, volume 20, 216 – 221.

Kerwin, W.J., Huelsman, L.P., and Newcomb, R.W. (1967). State-Variable Synthesis for Insensitive Integrated Circuit Transfer Functions. *IEEE J. Solid-State Circuits*, 2(3), 87–92.

Leang, K.K. and Devasia, S. (2006). Design of hysteresis-compensating iterative learning control for piezo positioners: application to atomic force microscopes. *Mechatronics*, 16(3–4), 141 – 158.

Leyva-Ramos, J., Escobar, G., Martinez, P.R., and Mattavelli, P. (2005). Analog circuits to implement repetitive controllers for tracking and disturbance rejection of periodic signals. *IEEE Trans. Circuits Syst. II, Exp. Briefs*, 52(8), 466–470.

Merry, R.J.E., Ronde, M.J.C., van de Molengraft, R., Koops, K.R., and Steinbuch, M. (2011). Directional repetitive control of a metrological AFM. *IEEE Trans. Cont. Sys. Tech.*, 19(6), 1622 – 1629.

Moore, K.L., Dahleh, M., and Bhattacharyya, S.P. (1992). Iterative learning control: a survey and new results. *Journal of Robotic Systems*, 9(5), 563–594.

Raffel, C. and Smith, J. (2010). Practical Modeling of Bucket-Brigade Device Circuits. In *Proc. 13th International Conference on Digital Audio Effects (DAFx-10)*. Graz.

Salapaka, S.M. and Salapaka, M.V. (2008). Scanning probe microscopy. *IEEE Control Syst. Mag.*, 28(2), 65 – 83.

Sangster, F.L.J. and Teer, K. (1969). Bucket-brigade electronics: new possibilities for delay, time-axis conversion, and scanning. *IEEE J. Solid-State Circuits*, 4(3), 131–136.

Shan, Y. and Leang, K.K. (2012a). Accounting for hysteresis in repetitive control design: nanopositioning example. *Automatica*, 48(8), 1751 – 1758.

Shan, Y. and Leang, K.K. (2012b). Dual-stage repetitive control with Prandtl-Ishlinskii hysteresis inversion for piezo-based nanopositioning. *Mechatronics*, 22, 271 – 281.

Skogestad, S. and Postlethwaite, I. (2005). *Multivariable Feedback Control: Analysis and Design*. Wiley-Interscience.

Walden, R.H. (1999). Analog-to-digital converter survey and analysis. *IEEE J. Sel. Areas Commun.*, 17(4), 539–550.

Weckler, G. (1977). Bucket Brigade Devices Circa 1977. In *Charge Transfer Device Signal Processing – A Short Course Organized by M. H. White*. The American University.

Wu, Y. and Zou, Q. (2007). Iterative control approach to compensate for both the hysteresis and the dynamics effects of piezo actuators. *IEEE Trans. Control Syst. Technol.*, 15(5), 936 – 944.